Ma Zhenhe (Orcid ID: 0000-0003-4079-9550)

Simultaneous detection of cerebral blood perfusion and cerebral edema using swept-source optical coherence tomography

Jian Liu [a], Yan Li [a], Yao Yu [a], Xincheng Yuan [b], Hongyu Lv [c], Lanxiang Liu[d], Yuqian Zhao [a], Yi Wang [a] and Zhenhe Ma [a,*]

[a] *School of Control Engineering, Northeastern University at Qinhuangdao, Qinhuangdao 066004, China*

[b] *Department of Biomedical Engineering, University of Michigan, Ann Arbor, MI, USA.*

[c] *Department of Ophthalmology, Maternal and Child Health Hospital, Qinhuangdao, China*

[d]*Department of Magnetic Resonance Imaging, Qinhuangdao Municipal No. 1 Hospital, Qinhuangdao, China*

**Corresponding author: mazhenhe@163. Com*

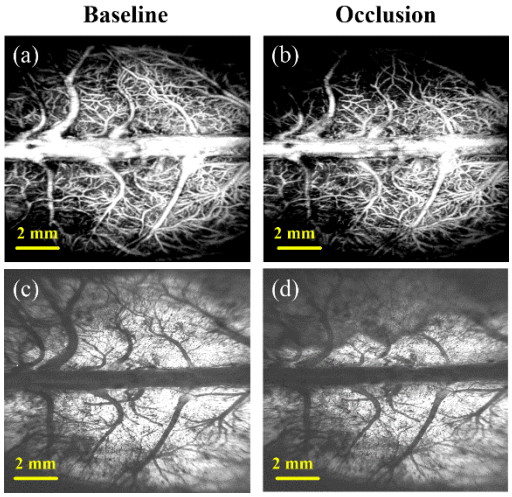

Graphical abstract: Simultaneous detection of cerebral blood perfusion and cerebral edema in middle cerebral artery occlusion (MCAO) rats using SS-OCT. *En face* OCT angiogram at baseline (a) and during occlusion (b), and *En face* attenuation coefficient maps at baseline (c) and during occlusion (d) can be used to quantify vascular perfusion density levels and brain edema state, respectively.

Abstract: The progression of ischemic cerebral edema (CE) is closely related to the level of cerebral blood perfusion (CBP) and affects each other. Simultaneous detection of CBP and CE is helpful in understanding the mechanisms of ischemic cerebral edema development. In this article, a wide field of view (FOV) SS-OCT system was used to detect CE status and CBP levels simultaneously in middle cerebral artery occlusion (MCAO) rats. Images reflecting these two physiological states can be reconstructed

This is the author manuscript accepted for publication and has undergone full peer review but has not been through the copyediting, typesetting, pagination and proofreading process, which may lead to differences between this version and the Version of Record. Please cite this article as doi: 10.1002/jbio.201960087

with only one C-scan. We quantify these two physiological states into 4 parameters, which contain two vascular parameters (vascular displacement distance and vascular perfusion density) and two edema parameters (optical attenuation coefficient and edema area). The association between the two vascular parameters and the two edema parameters were analyzed. The results show that there is a strong linear relationship between blood flow parameters and edema parameters. This work provides a new option for CE *in vivo* detection, and is very likely to play an important role in the development of relevant drugs or in selection of treatment options.

Keywords: swept-source optical coherence tomography, cerebral edema, cerebral blood perfusion, middle cerebral artery occlusion, optical attenuation coefficient

Introduction

Malignant ischemic stroke has a disproportionately high mortality rate due to the rapid development of refractory space-occupying cerebral edema (CE) [1]. Studies have shown that once CE is formed, cellular metabolite concentration will alter immediately and followed by cellular physiology, biochemistry and function. More importantly, swollen brain tissue can squeeze peripheral blood vessels, causing peripheral brain tissue ischemia, which will form a vicious circle of “ischemia - edema - re-ischemia - re-edema ", and eventually triggers cerebral herniation and endangers patients' lives [2]. This shows that the progression of ischemic CE is closely related to the level of cerebral blood perfusion (CBP) and affects each other. However, most of the existing research on simultaneous analysis of CBP and CE is carried out using different equipment or techniques [3, 4]. The two physiological parameters are usually obtained at different times, which make it difficult to effectively study the correlation and transformation

law between the two. If there is a device that can simultaneously monitor and quantify CBP and CE, it will be substantially helpful in providing more and deeper insights into the mechanism for ischemic CE development.

Basic research on animal models is able to help reveal the pathogenesis of a disease, for which develop new drugs, or evaluate the effectiveness of new treatment strategies. Therefore, *in vivo* imaging studies for small animals are equally important. In view of their high genetic similarity with humans, rapid reproduction, and low cost, both rats and mice have been wildly used as experimental subjects by researchers [5]. However, compared with mice, rats have more tenacious vitality, lower mortality, and longer abdominal anesthesia; under the safe dose, rats can be anesthetized for 2 hours, while mice for only 20 minutes. Therefore, the rat model is more suitable for our experiment.

Animal computed tomography (CT) [6, 7] and high resolution animal magnetic resonance angiography (MRA) [8] are commonly used imaging techniques in animal research, which have the advantages of non-contact and no imaging depth limitation. However, they also have shortcomings. In terms of CBP detection, their resolution is not sufficient to show the microcirculation of the brain (the capillary diameter is about 6-9 μm). In the detection of CE, they are not sensitive enough and are consequently not suitable for detection at early stages. For example, CT detects CE by capturing the effacement of the cerebral sulci and gyri. However, these findings are observer-dependent [9, 10]. T2-Weighted Resonance Imaging (T2WI), an MRI sequence, can only detect vasogenic edema after the end of the treatment time window [11]. Diffusion-weighted imaging (DWI), another sequence of MRI, is capable of detecting changes in the apparent diffusion coefficient (ADC) of water, which cytotoxic edema is sensitive

to [12]. Although promising, DWI has the disadvantage of poor resolution, which only allows detection of focal lesions larger than a few millimeters;

Optical coherence tomography (OCT) is a non-invasive imaging modality that allows volumetric imaging of living biological tissues with high spatial and temporal resolution [13~16]. Since its invention in 1990s, OCT technique evolved from the original temporal domain OCT (TD-OCT) to the Fourier domain OCT (FD-OCT). The latter includes Spectral Domain OCT (SD-OCT) and Swept Source OCT (SS-OCT). In recent years, with the continuous improvement of swept lasers, the sweeping rate of SS-OCT has significantly increased from hundreds kHz to MHz or even multi-MHz [17,18]. Thanks to its higher light intensity and higher spectral resolution, SS-OCT is better able to cope with rugged samples in wide field of view (FOV) imaging. In addition to the microstructural imaging capability, OCT can also be utilized to provide 3D blood angiography down to capillary level and attenuation coefficient imaging in tissue beds *in vivo* using methods called OCT-based angiography (OCTA) [19] and OCT-based attenuation imaging (OCT-AI) [20~22], respectively. Over the past few years, OCTA technique has been intensively used to study *in vivo* microvasculature of a variety of biological tissues in preclinical and clinical settings, such as animal brain [23], human retina [24], skin [25], even the mouth and nose [26]. OCT-AI, which calculates the optical attenuation coefficient (OAC) from the OCT signal to distinguish different tissue types or pathological states (including CE), which is receiving more and more attention [27,28]. A recent study showed that OAC is affected by the water content of brain tissue. The transmittance of near-infrared light increases (i.e. OAC decreases) when edema occurs in brain tissue. Such change is due to the presence of acidic substances in the edema cells, which increases the permeability of the cell membrane

[29]. In another study, a "water poisoning model" was used, which was made by intraperitoneal injection of excess physiological saline into mice. Excessive water penetrates into the brain over time, and the water content of the brain cells gradually increases, which in turn forms CE. They used SD-OCT to detect OAC at different locations in the cerebral cortex, and found that the average OAC of the cerebral cortex gradually decreased as CE progressed [30]. They also analyzed cerebral blood flow using Doppler OCT techniques and found that cerebral blood flow slowed during late-stage edema. However, simultaneous detection of CBP and CE using SS-OCT in middle cerebral artery occlusion (MCAO) animals has not been reported.

In this article, a wide-FOV SS-OCT system was used to detect CE status and CBP levels simultaneously in MCAO rats. Images reflecting these two physiological states can be reconstructed with only one C-scan (a set of 3D data). We quantify these two physiological states into 4 parameters (two vascular parameters and two edema parameters). Vascular parameters include “vascular displacement distance” and “vascular perfusion density”. Edema parameters include “OAC value” and “edema area”. We analyzed the association between the two vascular parameters and the two edema parameters. Some preliminary results were obtained. This work provides a new option for CE *in vivo* detection, and is very likely to play an important role in the development of relevant drugs or in selection of treatment options.

Method

Animal Model

In this study, three-month-old Sprague-Dawley rats (male) were used, each weighing approximately 280 g (Beijing Vital River Laboratory Animal Technology Co., Ltd. China). All procedures were performed in accordance with the Animal Ethics and

Administrative Council of Northeastern University. All efforts were made to minimize animal suffering and to reduce the number of animals used. Surgical anesthesia was induced with sodium pentobarbital (3%, 5 mg/100 g, IP). The anesthetized rats were fixed on a stereotaxic apparatus (ST-5ND-C) with ear bars and a clamping device. During the experiment, the body temperature of the animal was maintained at 36.8 ℃ using a homoeothermic blanket system. To obtain a clearer image, we ground the skull to a suitable thickness using a 1.2 mm diameter flat cranial drill. After the procedure, the rat was placed in the arm of the OCT sample and prepared for data acquisition (baseline).

The model of cerebral ischemia used in our experiments was based on endothelin-1-induced MCAO model described previously [31]. The stereotaxic coordinates of the ET-1 (Shanghai Jianglai industrial Limited by Share Ltd. China) injection were 0.9 mm anterior, 5.2 mm lateral and 8.7 mm ventral relative to bregma. A dose of 3μl ET-1 (60 pmol/L diluted with saline) was injected at 1μl/min. After injection, we waited 3 mins to ensure that the drug was fully absorbed. The needle was slowly removed and the rat was immediately placed under the sample arm for scanning.

System

A wide-range SS-OCT system was used for the experiments, as shown in Fig.1. Briefly, the light source employed is a swept-source with a central wavelength of 1310 nm and a bandwidth of 100 nm. The system operating at 200 kHz swept rate and providing an axial resolution of ~7.5 μm in air. The use of a 50-mm focal length objective lens makes the system to achieve the lateral resolution of ~16 μm. Although, the theoretical ranging depth of the system can reach ~78 mm, we digitized each interference spectrum to 5,000 points in this paper, which provided an actual measurement depth of ~16 mm.

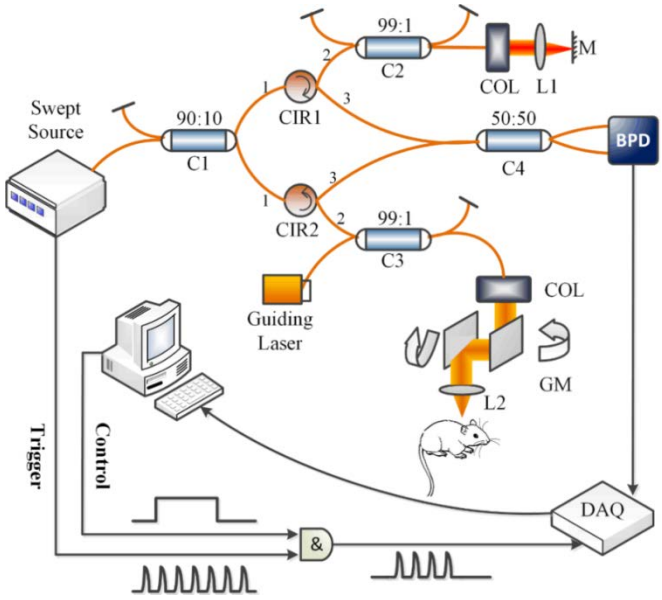

Fig.1. Wide-range Swept-Source OCT system. L1, L2: Lens; C1, C2, C3, C4: Fiber Coupler; BPD: Balanced Photo Detector; M: Mirror; COL: Collimator; CIR1, CIR2: Circulator; GM: Galvanometric mirror.

OCTA protocol

OCTA utilizes the intrinsic motion contrast caused by dynamically moving particles (e.g. red blood cells) to differentiate functional blood vessels from static tissue background. In our system, the fast scanner (X direction) was driven by a saw tooth waveform with a 160 Hz frame rate, providing 6.25 ms time interval between adjacent repeated B-scans. Each B-scan image contained 1000 A-lines that occupied 80% duty cycle. The slow scanner (Y direction) was driven by a step function waveform, which led to 800 B-scan positions with 4 repeated B-scans per step. The FOV is 12 mm (X direction) ×10 mm (Y direction), enough to cover the entire cerebral cortex of the rats. Therefore, each data set of the OCTA contained 3,200,000 A-lines, taking 20 seconds to complete the data acquisition. To obtain the signals representing the blood flow, a differential operation of the repeated B-scans on each cross-section was applied to eliminate the static tissue signals.

Motion artifact elimination

Performing image registration for repeated B-scans at the same location is an effective way to eliminate motion artifacts. In this paper, an image registration algorithm based on constrained demons introduced in our previous research was used [32]. We collected 4 B-scans at each position, use the first B-scan as the reference image, and register the next three B-scans with the first B-scan. Before the registration is executed, we first calculate the correlation coefficient between the reference image and the image to be registered, and then use the appropriate threshold. Only the frames with their correlation coefficient smaller than the threshold are selected to perform registration. In this paper, we set the threshold to 92%.

Quantification of vascular perfusion density

The vascular perfusion density (VPD), defined as the ratio of "pixels of blood vessels with flow" to "pixels of the entire blood vessel image", is an indicator of cerebral perfusion level. In this paper, VPD was calculated using “locally adaptive region growing” algorithm proposed previously [33]. Briefly, the algorithm consists of four steps: 1) The selection of initial seed pixels; 2) Local region selection; 3) Threshold update; 4) Similarity judgment. Firstly, initial seed pixels were automatically selected with a certain gray value in an image histogram. Then, a local region around the initial seed pixel was determined based on vessel size, and a threshold was calculated based on the value of seed pixels. Within the neighborhood of the initial seed pixel, candidate pixels with similarity are incorporated into the object region (here, the object region represents a blood vessel). The similarity here indicates that the difference between two pixels is less than the constantly updated threshold. Based on this growth condition, the algorithm was repeated and terminated when there were no absorbable pixels.

Elimination of confocal interference

The signal intensity of OCT is affected by the distance between the detected position and the focal plane. The closer to the focus, the stronger the signal intensity is; on the contrary, the weaker. This characteristic seriously affects the accurate calculation of OAC. Faber et al. derived the general expression of the confocal axial point spread function (PSF) [34, 35]. The influence of confocal characteristics could be removed by dividing the axial PSF. In this paper, we adopted this method.

Calculation of optical attenuation coefficient (OAC)

Before OAC calculation, we performed surface extraction and flattened the image. Then, a 3D matrix was reconstructed from the cortex surface, extending a specific number of pixels vertically. An optimized depth-resolved estimation (ODRE) method was used to calculate optical attenuation coefficient (OAC) [36]. This method can accurately calculate the OAC at any depth. Briefly, under the condition that the backscattered light reflected towards photo detector of the OCT system is a fixed fraction of the attenuated light, each pixel in the OCT dataset is converted into a corresponding OAC pixel using the following relationship:

$$\mu[z] = \frac{I[z]}{2\Delta \sum_{i=z+1}^{N} I[i] + \frac{I[N]}{\mu[N]}} \tag{1}$$

where $I[z]$ is the OCT signal of a pixel and $\mu[z]$ is the OAC, both at depth z, Δ is the pixel size (usually related to the axial resolution of the OCT system). N is the number of the pixels within a limited depth. $I[N]$ is the OCT signal for the last point N. $\mu[N]$in Eq. (1) is unknown. To determine it, a piece of data (120 pixels) was taken from the end of the imaging depth and then fitted to an exponential curve. The fitting model

is $y = a \cdot \exp(-2\mu z) + b$ .The fitted result μ is the average attenuation coefficient of this data and can be considered as the best approximation of $\mu[N]$. After exponential fitting, we bring the μ into Eq. (1). When all the A-scan calculations are completed, a set of 3D OAC matrices is obtained.

Entire process of OCT data processing

The entire process of OCT data processing is summarized in Fig. 2.

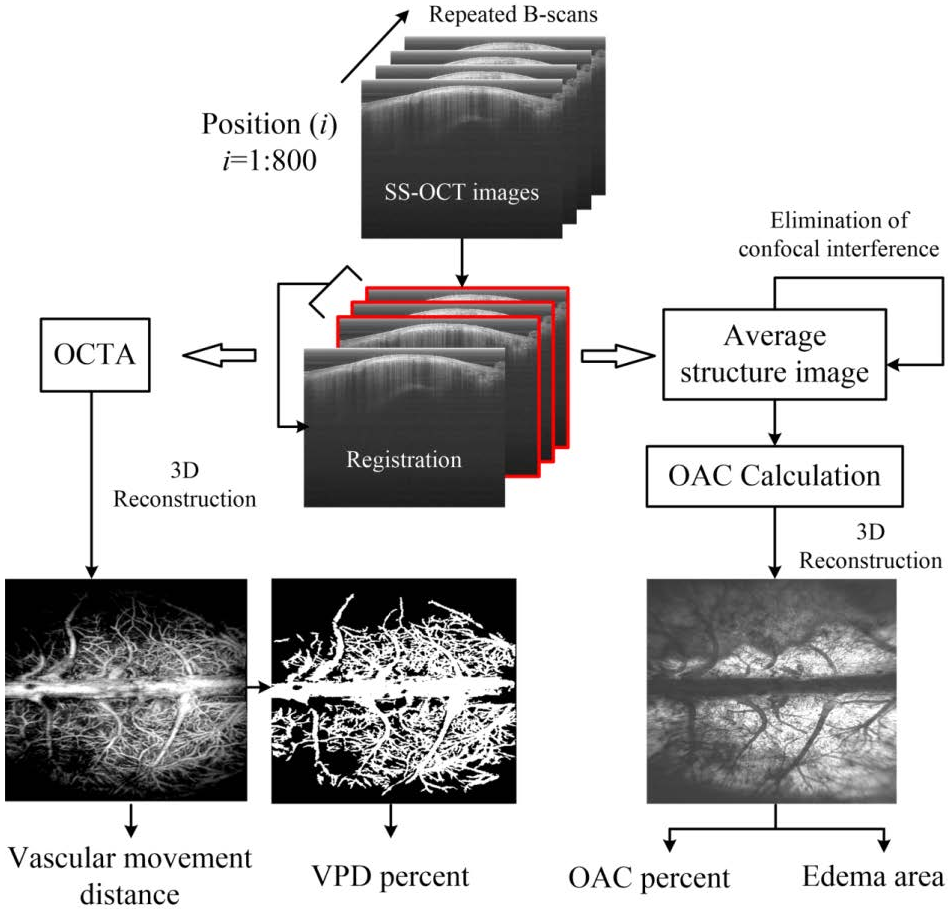

Fig. 2 The entire process of OCT data processing. First, the initial OCT structure images obtained by the SS-OCT were registered. Then, 2D angiograms at different locations were obtained by the difference of repeated B-scans, and the 3D angiograms were reconstructed by Amira software. By comparing the angiograms at baseline and occlusion, the vascular displacement distance can be obtained. The percentage change of VPD was calculated using “locally adaptive region growing algorithm”. On the other hand, by averaging the repeated B-scans, we were able to obtain average

structural images. The influence of confocal characteristics was removed by dividing by the axial PSF proposed by Faber et al. An ODRE method was used to the calculation of OAC. A series of *en face* OAC maps were obtained by averaging the OACs in the specific depth range. Last, the percentage change of OACs and the edema areas were obtained from the *en face* OAC map.

Result

With a single C-scan, we can quantify four parameters: vascular displacement distance, VPD, OAC and edema area. Figure 3 shows the calculation process of the vascular displacement distance.

When ischemic CE occurs, the swollen brain tissue will squeeze the surrounding blood vessels, causing a further reduction in brain blood supply. The blood vessels will move as they are squeezed by the edema tissue. Quantification of the resultant vascular displacement distance can indirectly help evaluate the degree of tissue expansion. Fig. 3(a) shows *en face* maximum intensity projection (MIP) of the vascular network in cortical layers of a rat brain (up to 300μm depth) at the baseline. Fig. 3(b) is the angiogram after occlusion (60 min after MCAO). Figures 3(c) and (d) are magnified partial areas in (a) and (b), respectively. Shown as the yellow box in (b). The red boxes in (c) and (d) provide a visual reference to see the apparent displacement of some blood vessels (indicated by the red arrow). By comparing the angiograms at baseline and occlusion, the vascular displacement distance can be obtained.

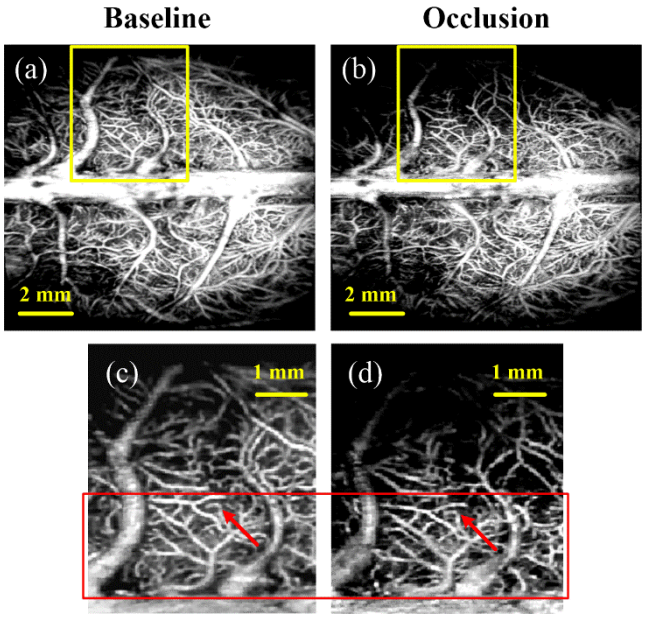

Fig. 3 Schematic diagram of vascular displacement. (a) OCT angiogram at baseline. (b) OCT angiogram during occlusion. (c) (d) Closer view of a region marked by a solid yellow box in (a) and (b). The red rectangle represents a region where vascular displacement is observable while the red arrows indicate vessels of that type.

In terms of quantification of CBP levels, we used vascular perfusion density (VPD) as the indicator. Due to individual differences, there may be a large gap between VPDs in different rats. Therefore, we used the ratio of post-occlusion VPD to that at baseline to describe the degree of ischemia for each individual of MCAO rat. Fig.4 shows the vascular segmentation results corresponding to fig.3. VPD was calculated based on the segmentation results. In fig. 4 (c), the left y-axis shows the VPD at the baseline and occlusion, respectively, and the right y-axis shows the percentage change of VPD.

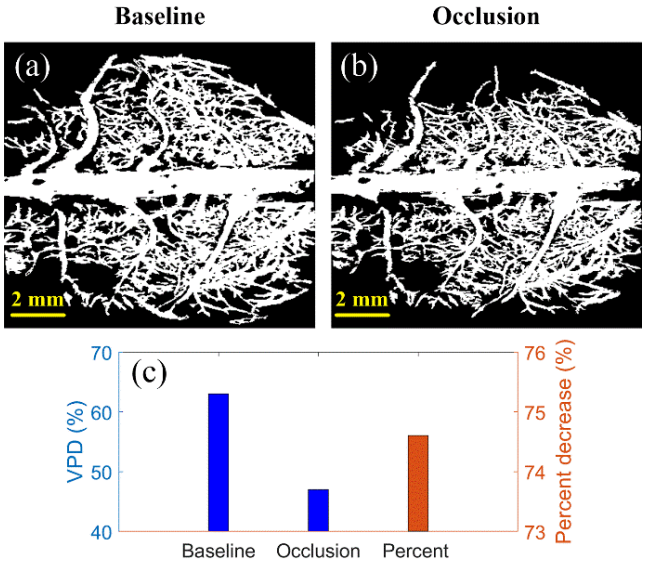

Fig. 4 Quantification of VPD. Blood vessel segmentation results using 'locally adaptive region growing' algorithm at baseline (a) and during occlusion (b), respectively. (c) Quantized VPD. The percentage of VPD before and after occlusion is denoted by the y-axis on the right of the graph.

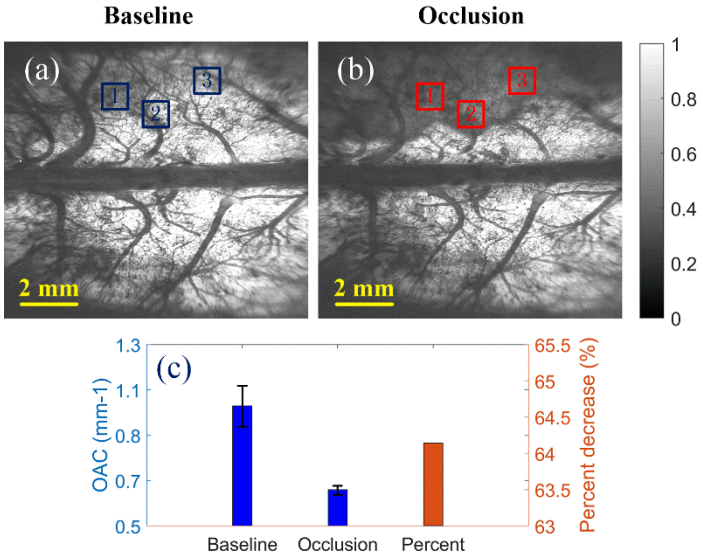

Fig. 5 *en face* OAC maps at baseline (a) and during occlusion (b). Three 20×20 pixel regions on the baseline image (blue square 1.2.3) and the occlusion image (red square 1.2.3) were selected to observe changes in OAC. (c) OAC values. All values are reported as the mean ± S.E.M. The percentage of averaged OAC before and after occlusion is denoted by the y-axis on the right of the graph.

Similar to VPD percentage, we used OAC percentage to describe changes in the attenuation coefficient of brain tissue. We reconstructed *en face* OAC images by averaging the OACs within the depth range of 0.7~2.5 mm. The reconstruction results are shown in Fig. 5. We selected three 20×20 pixel regions on the images at baseline and occlusion respectively, shown in blue square 1.2.3 in fig.5 (a), and red square 1.2.3 in fig.5 (b). The averaged OAC values are shown in fig.5 (c). The right y-axis shows the percentage change of the averaged OAC value.

We also segment the shaded area from the *en face* OAC images manually, as shown by the red dashed line in fig. 6(a), and calculate the area of the shadow. In this paper, 5 rats were used and the quantification of edema area in different rats is shown in fig. 6(b). The edema area, obviously, is able to directly reflect the degree of brain tissue swelling. As for treatment of CE with certain drugs or other treatment strategies, the edema area provides the most intuitive reflection of their efficacy. All of the four parameters in five rats are listed in Table 1.

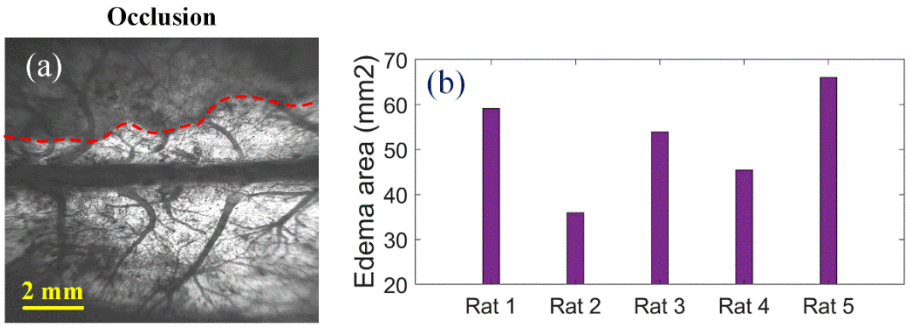

Fig. 6 (a) Edema area quantification. The red dotted line marks the area where the OAC dropped significantly. (b) Edema area in five rats.

Tab. 1 Four parameters in five rats

Parameter	Rat 1	Rat 2	Rat 3	Rat 4	Rat 5

Vascular movement distance (mm)	0.15	0.09	0.14	0.11	0.2
VPD percentage (%)	64.4	75.9	74.6	71.5	65.8
OAC percentage (%)	57.1	77	64.2	60	52.6
Edema area (mm^2)	59.1	35.9	53.9	45.4	66

We paired two vascular parameters and two edema parameters into four combinations: Vascular movement distance *vs* OAC percentage, vascular movement distance *vs* edema area, VPD percentage *vs* OAC percentage, and VPD percentage *vs* edema area. The linear relationship between them was analyzed and some preliminary results were obtained. As shown in Figure 7.

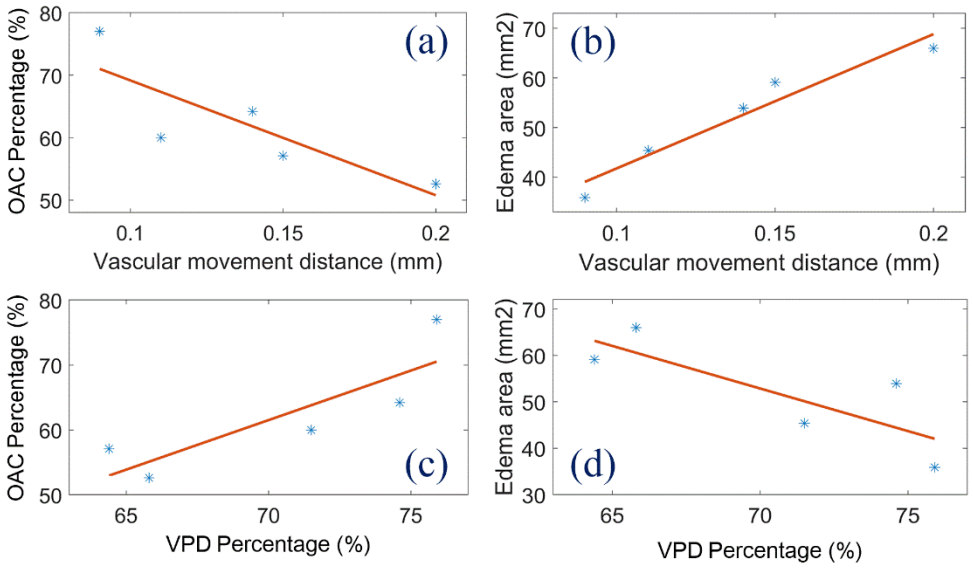

Fig. 7 Linear relationship between two vascular parameters and two edema parameters. (a) vascular movement distance *vs* OAC percentage, (b) vascular movement distance *vs* edema area, (c) VPD percentage *vs* OAC percentage and (d) VPD percentage *vs* edema area.

From the results, we can see that there is a linear relationship between vascular parameters and edema parameters, no matter which combination of the two parameters.

Vascular movement distance is inversely proportional to OAC percentage, and proportional to edema area; The VPD percentage is proportional to OAC percentage, and inversely proportional to edema area. Among them, vascular movement distance has the closest relationship with edema area.

Discussion

In the pathogenesis of ischemic stroke, refractory CE is often accompanied, and its state is closely related to the level of CBP. If the two cannot be taken care of during the treatment, it is difficult to achieve the desired therapeutic effect [37]. For example, in the treatment of ischemic stroke, if we focus only on restoring CBP and ignoring CE, CBP may be reduced again due to the occupancy effect of CE; conversely, focus only on reducing CE while neglecting to restore CBP, CE may be further aggravated by the decrease of CBP.

The development of human medical standards is inseparable from the advancement of medical imaging technology. A synchronous imaging technique of CBP and CE is likely to bring unimaginable progress in the treatment of CE. In this paper, we monitored the CBP levels and CE status simultaneously in MCAO rats for the first time.

In our previous work, we monitored the OAC in MCAO rats using SS-OCT system, and found that the OAC in the deep cortical region in ischemic hemisphere decreases significantly over time, forming a shaded area. This area is highly consistent with MRI results, indicating the formation of CE. In this experiment, we found that blood flow immediately decreased after ET-1 injection. But at this time, OAC did not change significantly. After a period of ischemia, the OAC in the ischemic area began to

decrease significantly, and a low signal area appeared. As the low signal area gradually enlarged, the surrounding blood vessels were squeezed and displaced.

By using wide-field SS-OCT, we obtained two vascular parameters and two edema parameters with only one scan. The linear relationship between the two vascular parameters and the two edema parameters was analyzed separately. From the analysis results, we can see that the vascular displacement distance has the most direct relationship with the edema area. This may be due to the fact that the displacement of the blood vessel is just made by the occupancy effect of CE. The decrease in OAC value reflects the severity of edema. In the ischemic hemisphere, the degree of damage to brain tissue in different regions may be inconsistent, resulting in differences in OAC values in different regions. We only averaged the OAC values at three locations and may not fully reflect the edema severity of the whole brain. The correlation between VPD and edema area was the weakest among the four groups, probably due to the large difference in blood flow compensation between different individuals. However, in general, there are certain links between vascular parameters and edema parameters, and they affect and promote each other.

In summary, the progression of ischemic CE is closely related to the level of CBP and affects each other. Simultaneous detection of these two physiological states is important for the study of the disease. Wide-field, high-quality imaging is conducive to the capture of lesions. SS-OCT is capable of detecting CBP and CE simultaneously, to make up for the shortcomings of existing detection techniques, and has the potential to play an important role in ischemic CE research.

Funding

This work was supported in part by National Natural Science Foundation of China (61771119, 61901100 and 81871029), Hebei Provincial Natural Science Foundation of China (H2018501087, H2019501010 and F2019501132). Fundamental Research Funds for the Central Universities (N182304008, N172304034 and N172304029). Technology Supporting Program of Hebei Province (17277718D)

Disclosures

The authors declare that there are no conflicts of interest related to this article.

Reference

[1] S. D. Treadwell, & B. Thanvi, *Postgraduate medical journal*, 2010. *86*1014, 235-242.

[2] P. K. Manwaring, K. L. Moodie, A. Hartov, K. H. Manwaring, R. J. Halter. *Anesthesia and analgesia*. 2013;1174:866.

[3] D. Martz, M. Beer, & A. L. Betz, *J Cereb Blood Flow Metab*. 1990. 103, 352-357.

[4] J. M. Simard, M. Chen, K. V. Tarasov, S. Bhatta, S. Ivanova, & L. Melnitchenko, N. Tsymbalyuk, G. A. West & V. Gerzanich. *Nature Medicine*, 2006. 124, 433-440.

[5] M. Hudsonshore, *Altern Lab Anim*, 2016. 446, 569-580.

[6] S. J. Schambach, S. Bag, V. Steil, C. Isaza, L. Schilling, C. Groden, M. A. *Stroke*. 2009; 404: 1444-1450.

[7] F. Zhao, J. Liang, X. Chen, J. Liu, D. Chen, X. Yang, J. Tian. *Medical & biological engineering & computing*. 2016;542-3:511-524.

[8] N. Beckmann, R. Stirnimann, D. Bochelen. *Journal of magnetic resonance*. 1999;1402:442-450.

[9] C. Cristia, M. L. Ho, S. Levy, L. W. Andersen, S. M. Perman, T. Giberson, ... & M. W. Donnino, *Resuscitation*, 2014. 8510, 1348-1353.

[10] N. Tomura, K. Uemura, A. Inugami, H. Fujita, S. Higano, & F. Shishido, *Radiology*, 1988. 1682, 463-467.

[11] A. Obenaus, & S. Ashwal, *Neuropharmacology*, 553, 271-280. 2008.

[12] M. D. Phillips, & R. A. Zimmerman, *Neuroimaging clinics of North America*, 1999. *9*1, 41-52.

[13] D. Huang, E. A. Swanson, C. P. Lin, J. S. Schuman, W. G. Stinson, W. Chang, ... & C. A. Puliafito, *science*, 1991. 2545035, 1178-1181.

[14] Z. Ma, R. K. Wang, F. Zhang, & J. Yao, *Proceedings of SPIE - The International Society for Optical Engineering*, 2005. 5630, 286-294.

[15] Z. Ma, S. Dou, Y. Zhao, C. Guo, J. Liu, Q. Wang, ... & Y. Wang, *Applied optics*, 2015. *54*31, 9253-9257.

[16] Z. H. Ma, Y. S. Ma, Y. Q. Zhao, J. Liu, J. H. Liu, J. T. Lv, & Y. Wang, *Applied optics*,

2017. *56*31, 8832-8837.

[17] J. Xu, C. Zhang, J. Xu, K. K. Y. Wong, & K. K. Tsia, *Optics letters*, 2014. *39*3, 622-625.

[18] J. Xu, X. Wei, L. Yu, C. Zhang, J. Xu, K. K. Y. Wong, & K. K. Tsia, *Biomedical optics express*, 2015. *6*4, 1340-1350.

[19] C. L. Chen, & R. K. Wang, *Biomedical optics express*, 2017. *8*2, 1056-1082.

[20] D. J. Faber, F. J. Van Der Meer, M. C. Aalders, & T. G. van Leeuwen, *Optics express*, 2004. 1219, 4353-4365.

[21] K. A. Vermeer, J. Mo, J. J. A. Weda, H. G. Lemij, & J. F. De Boer, *Biomedical optics express*, 2014. 51, 322-337.

[22] G. T. Smith, N. Dwork, D. O'Connor, U. Sikora, K. L. Lurie, J. M. Pauly, & A. K. Ellerbee, *IEEE Trans. Med. Imaging*, 2015. 3412, 2592-2602.

[23] Y. Jia, & R. K. Wang, *Journal of biophotonics*, 2011. *4*1‐ 2, 57-63.

[24] L. An, M. Johnstone, & R. K. Wang, *Journal of biomedical optics*, 2012. *17*11, 116018.

[25] U. Baran, L. Shi, & R. K. Wang, *Journal of biophotonics*, 2015. *8*1-2, 46-51.

[26] W. J. Choi, & R. K. Wang, *Biomedical optics express*, 2014.58, 2620-2634.

[27] U. Baran, Y. Li, & R. K. Wang, *Applied optics*, 2015. 5421, 6448-6453.

[28] U. Baran, W. Zhu, W. J. Choi, M. Omori, W. Zhang, N. J. Alkayed, & R. K. Wang, *Journal of neuroscience methods*, 2016. 270, 132-137.

[29] D. Liang, S. Bhatta, V. Gerzanich, and J. M. Simard, *Neurosurg*. 2007. Focus 22, E2

[30] C. L. Rodriguez, J. I. Szu, M. M. Eberle, Y. Wang, M. S. Hsu, D. K. Binder, & B. H. Park, *Neurophotonics*, 2014. 12, 025004.

[31] J. Liu, Y. Ma, S. Dou, Y. Wang, D. La, J. Liu, & Z. Ma, *Journal of biomedical optics*, 2016. *217*, 075014.

[32] J. Liu, N. Ding, Y. Yu, L. Liu, X. Yuan, H. Lv, ... & Z. Ma, *Journal of biophotonics*. 2019.

[33] Z. Ma, N. Ding, Y. Yu, Y. Ma, X. Yuan, Y. Wang, ... & J. Liu, *Applied optics*, 2018. *57*35, 10117-10124.

[34] T. G. van Leeuwen, D. J. Faber, & M. C. Aalders, *IEEE Journal of selected topics in quantum electronics*, 2003. *9*2, 227-233.

[35] F. J. van der Meer, D. J. Faber, J. Perrée, G. Pasterkamp, D. B. Sassoon, & T. G. van Leeuwen, *Lasers in Medical Science*, 2005.*20*1, 45-51.

[36] J. Liu, N. Ding, Y. Yu, X. Yuan, S. Luo, J. Luan, ... & Z. Ma, *Journal of biomedical optics*, 2019. *24*3, 035002.

[37] M. Walberer, N. Ritschel, M. Nedelmann, K. Volk, C. Mueller, M. Tschernatsch, & T. Gerriets, *Journal of Neurosurgery*, 2008. 1092, 287-293.

Graphical Abstract

In this article, a wide field of view (FOV) SS-OCT system was used to detect CE status and CBP levels simultaneously in middle cerebral artery occlusion (MCAO) rats. Images reflecting these two physiological states can be reconstructed with only one C-scan. We quantify these two physiological states into 4 parameters, which contain two vascular parameters and two edema parameters. The association between the two vascular parameters and the two edema parameters were analyzed. The results show that there is a strong linear relationship between blood flow parameters and edema parameters.

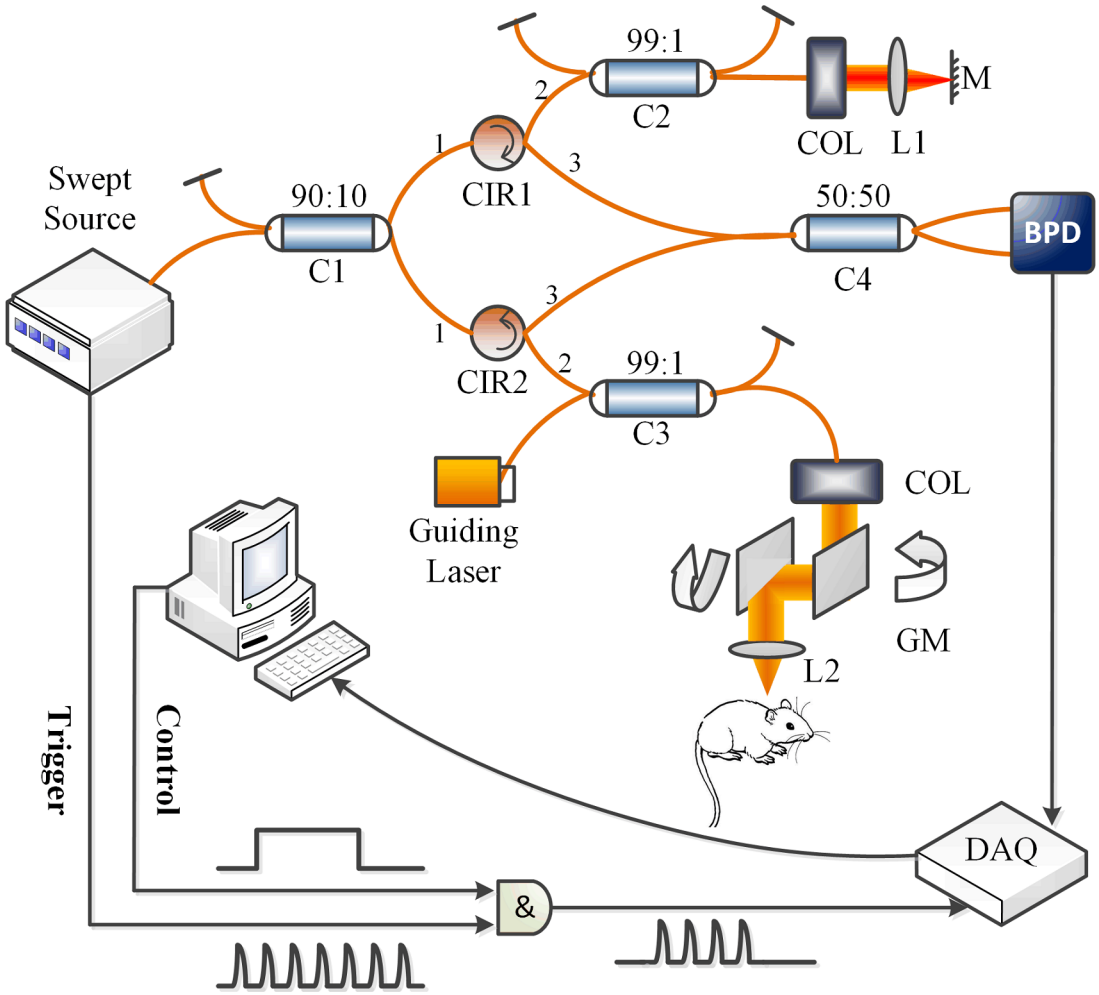

JBIO_201960087_Fig1.tif

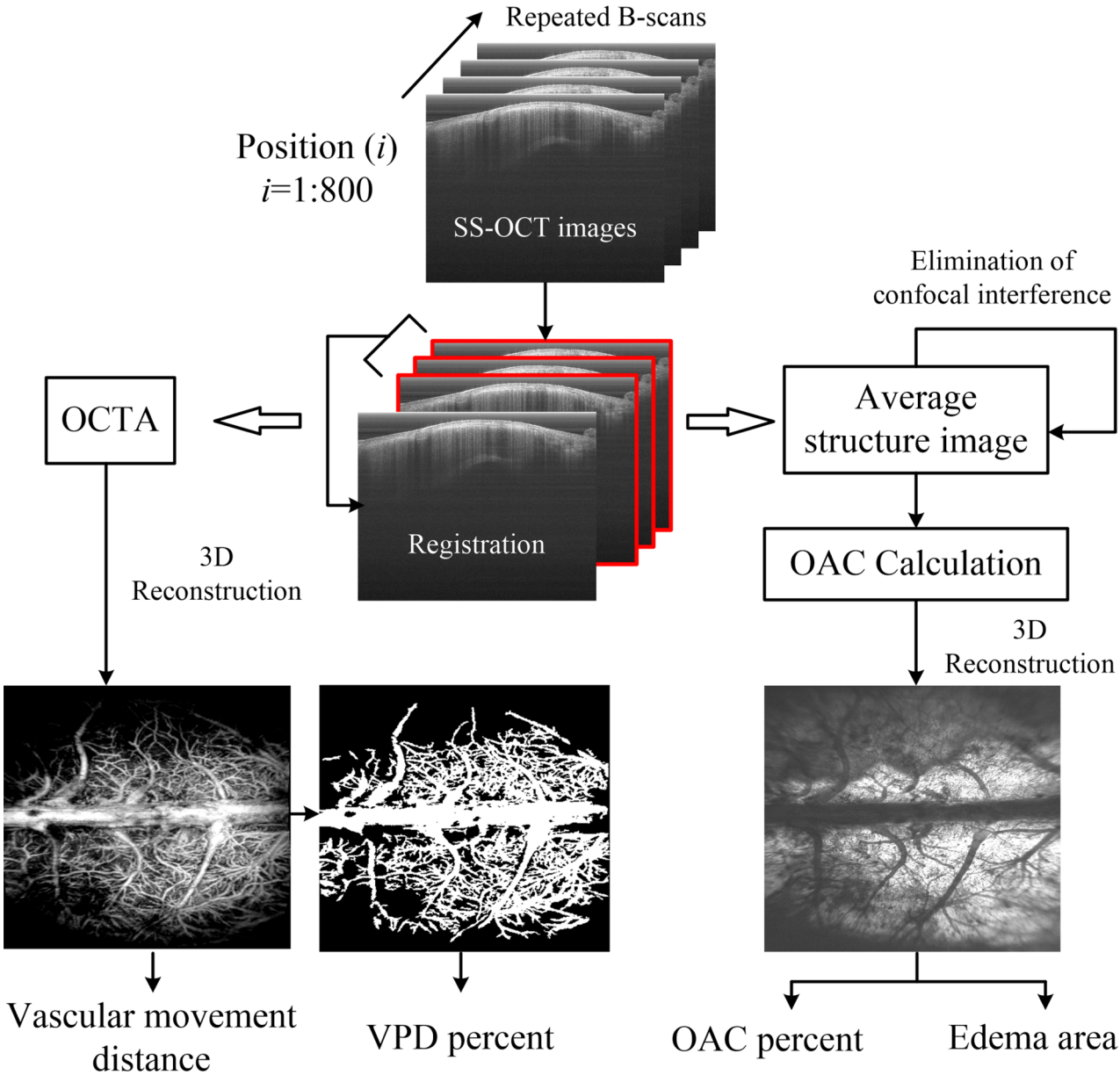

JBIO_201960087_Fig2.tif

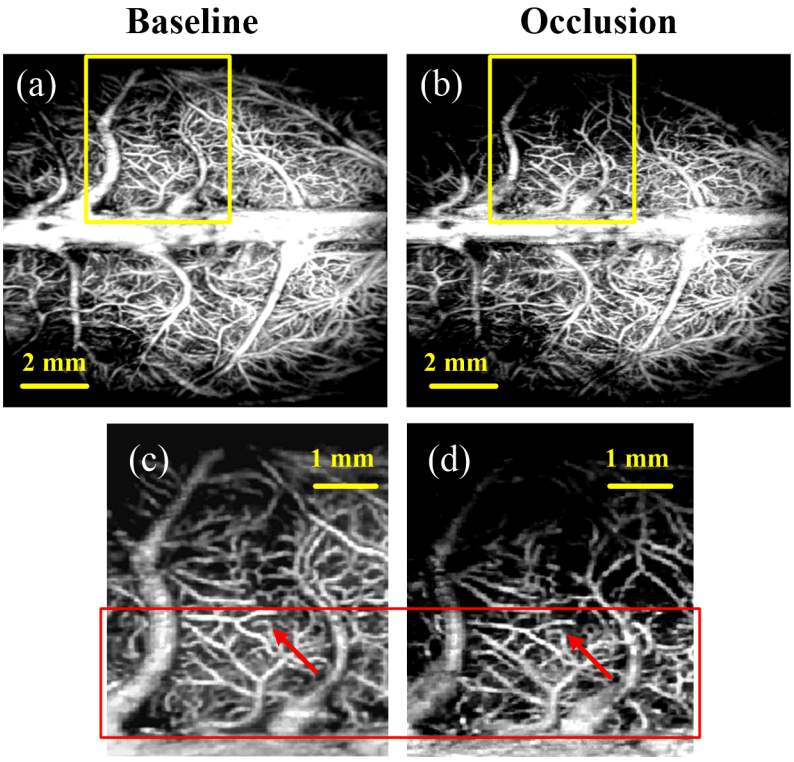

JBIO_201960087_Fig3.tif

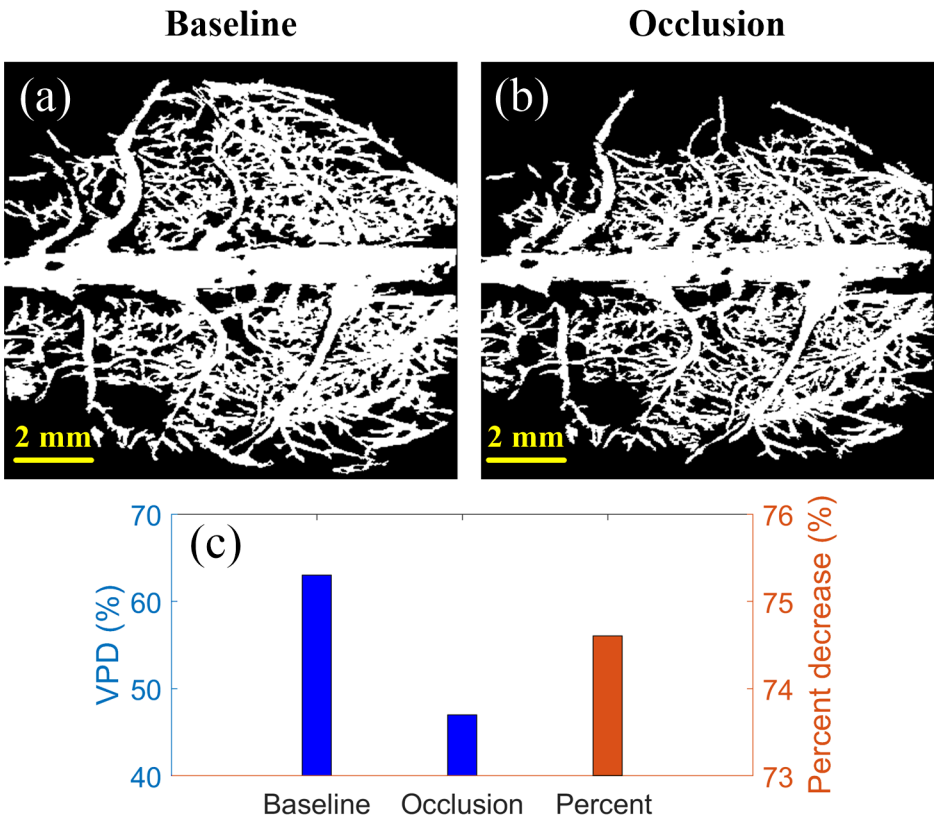

JBIO_201960087_Fig4.tif

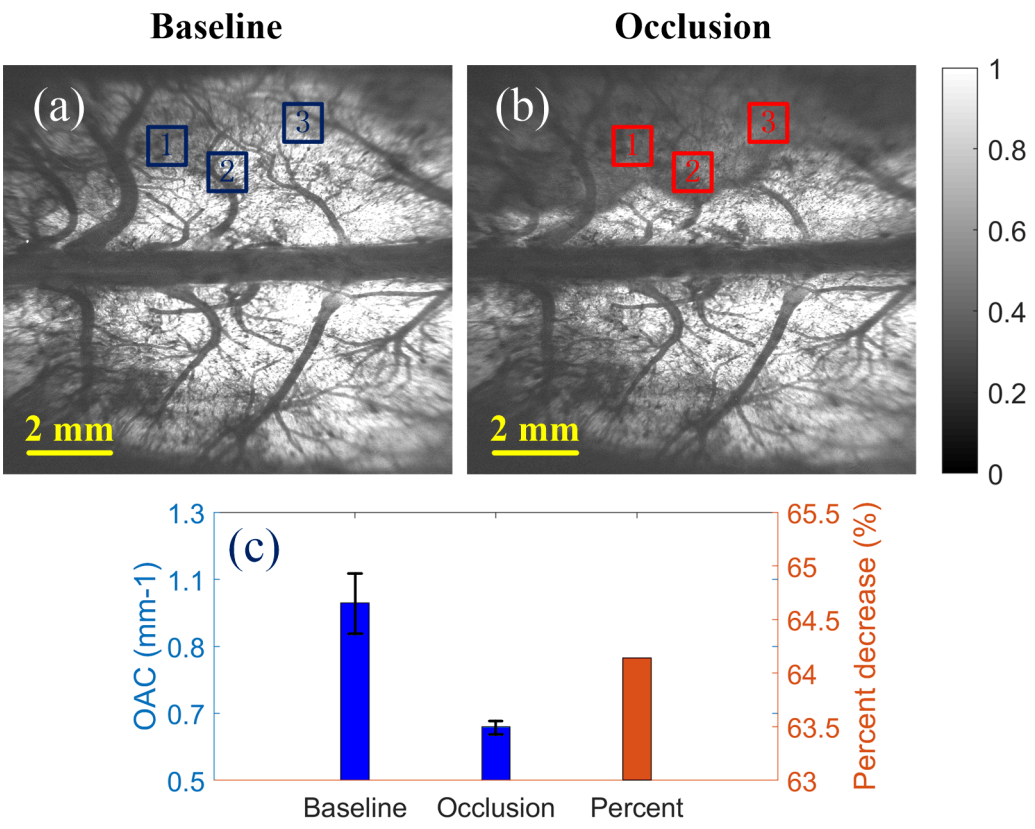

JBIO_201960087_Fig5.tif

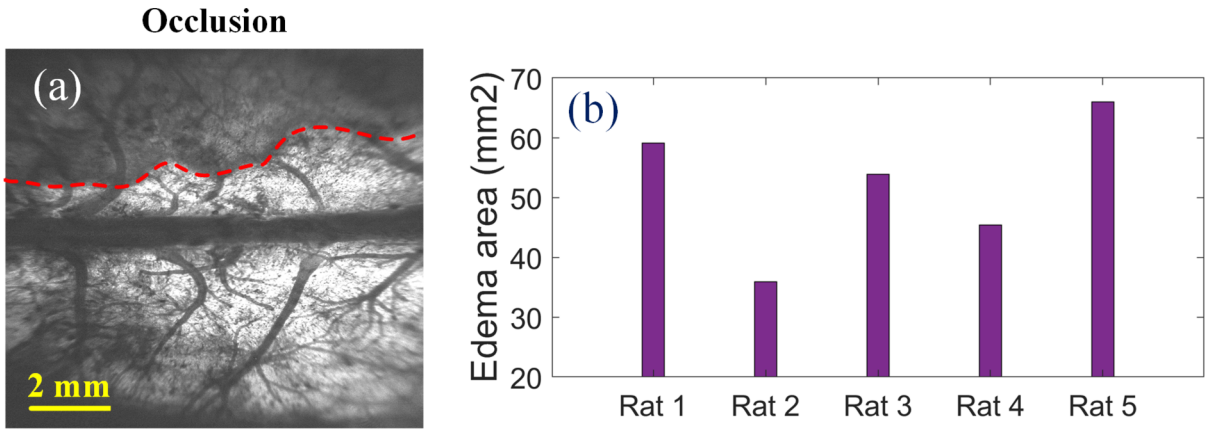

JBIO_201960087_Fig6.tif

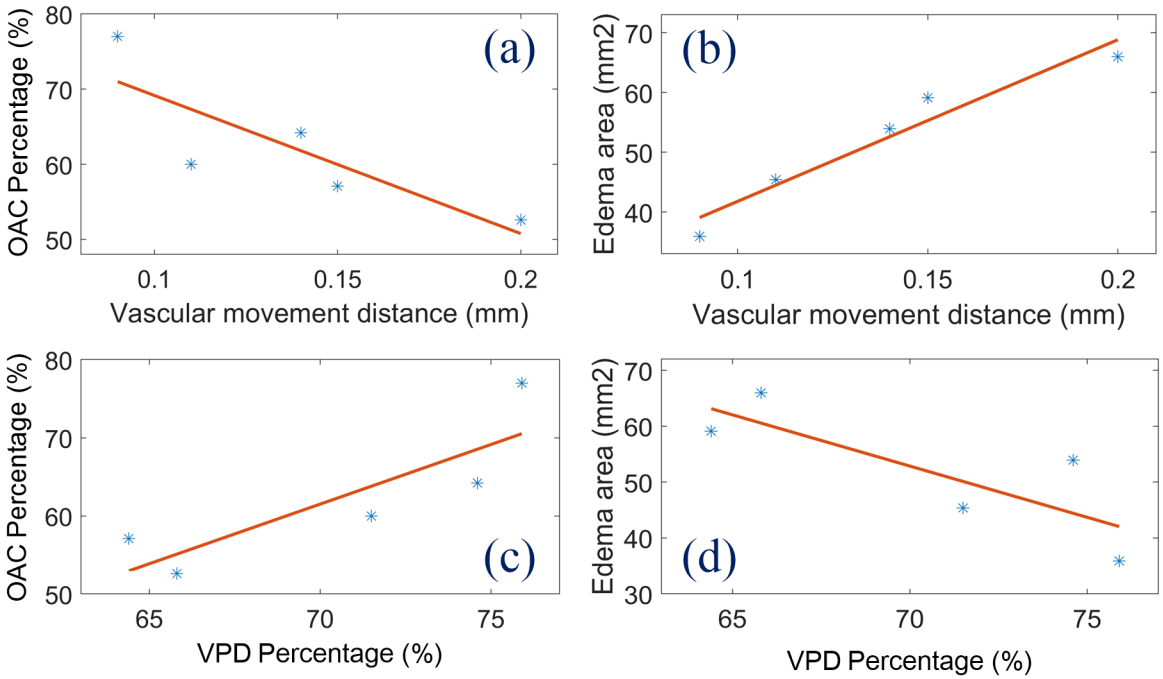

JBIO_201960087_Fig7.tif

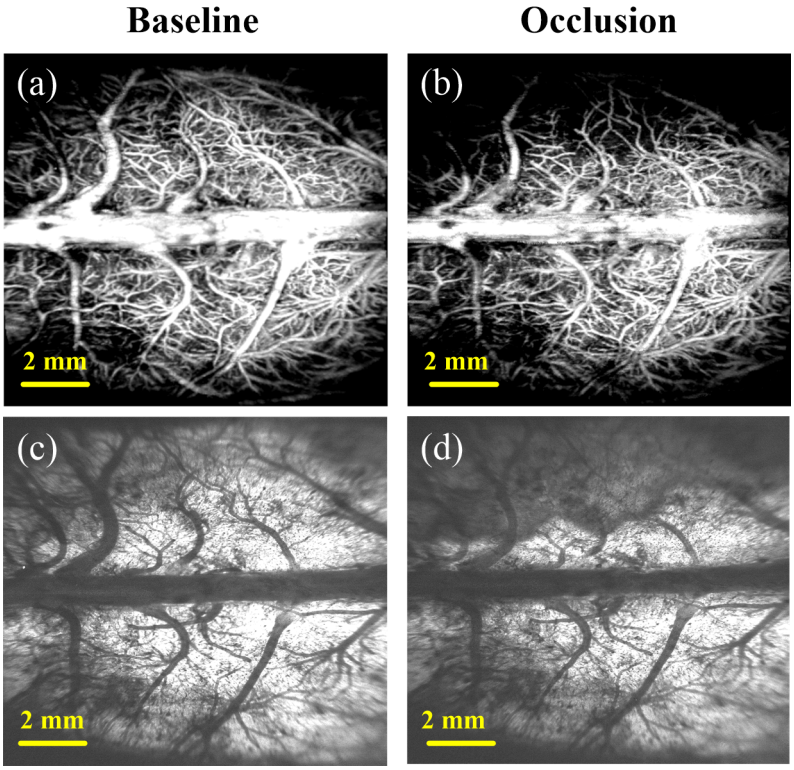

JBIO_201960087_graphical abstract.tif